



Compositional diversity and stratification of the Martian crust: Inferences from crystallization experiments on the picrobasalt Humphrey from Gusev Crater, Mars

Francis M. McCubbin,¹ Hanna Nekvasil,¹ Andrea D. Harrington,¹ Stephen M. Elardo,¹ and Donald H. Lindsley¹

Received 16 April 2008; revised 5 August 2008; accepted 22 August 2008; published 29 November 2008.

[1] Phase equilibrium experiments on a liquid composition of the Gusev Crater rock Humphrey (with added F and Cl) with 0.07 wt% and 1.67 wt% water have revealed the range in compositional diversity of lavas that could arise from fractionation at the base of a thick martian crust. Humphrey composition melts with 0.07 wt% water produce ne-normative alkalic residual melts at 9.3 kbar; silica progressively decreases with increasing degree of fractionation. This decrease in silica is accompanied by Fe-, Ti-, and P-enrichment. With 1.67 wt% bulk water content, Humphrey-like melts instead crystallize to produce residual melts that show progressive silica-enrichment, Al-enrichment, and Fe-depletion, progressing from mildly alkalic hy-normative basalt to trachyandesite. Coupled with the production of such residual liquids by fractionation is the formation of ultramafic to mafic cumulus lithologies that would remain at the base of the Martian crust. This process would lead to significant compositional stratigraphy of the crust that contains elements of both trends, as early hydrous primary magmas gave way to drier more depleted primary magmas upon dehydration of the magma source regions by repeated episodes of partial melting. The possibility of significant contribution of late silica-poor, Fe-enriched basalt, residual to fractionation at depth, to the present martian surface, makes it difficult to reliably use surface lithologies to constrain the compositional characteristics of the mantle magmatic source regions and the primary melts produced from them.

Citation: McCubbin, F. M., H. Nekvasil, A. D. Harrington, S. M. Elardo, and D. H. Lindsley (2008), Compositional diversity and stratification of the Martian crust: Inferences from crystallization experiments on the picrobasalt Humphrey from Gusev Crater, Mars, *J. Geophys. Res.*, 113, E11013, doi:10.1029/2008JE003165.

1. Introduction

[2] Much of our understanding of the nature and timing of the formation of the Martian crust comes from isotopic and trace element investigations of the shergottite meteorites. Various short- and long-lived isotope systems (¹⁴⁶Sm-¹⁴²Nd, ¹⁴⁷Sm-¹⁴³Nd, ¹⁸²Hf-¹⁸²W, ⁸⁷Rb-⁸⁷Sr, ¹⁸⁷Re-¹⁸⁷Os) confirm that Mars experienced a major silicate differentiation early (~4.5 Ga) and did not experience “major melting” after this time [Borg *et al.*, 1997, 2003; Brandon *et al.*, 2000; Foley *et al.*, 2005; Harper *et al.*, 1995; Kleine *et al.*, 2002, 2004; Lee and Halliday, 1997; Yin *et al.*, 2002]. As summarized by McLennan [2001, 2003] and Wieczorek and Zuber [2004], this early differentiation resulted in a primary Martian crust that was enriched in large-ion lithophile (LIL) elements and isotopically isolated from the depleted mantle. After formation of the primary crust, a secondary crust formed upon input of magmas from the depleted Martian mantle [Taylor, 2001;

Wieczorek and Zuber, 2004]; the extent of this secondary magmatism was likely dictated by the budget of heat-producing elements in the depleted mantle [McLennan, 2001].

[3] Relative thickness estimates for the primary and secondary crusts are under-constrained; however, upper and lower limits have been established. Wieczorek and Zuber [2004] reported that the Martian crust likely ranges in thickness from 33 to 81 km, although the nominal value of 57 km is typically used [Taylor *et al.*, 2006; Wieczorek and Zuber, 2004]. Norman [1999] estimated on the basis of rare earth elements (REEs) and Nd isotope concentrations (in SNC meteorites) that the thickness of the primary crust ranges from 10 to 45 km, although 20–30 km is most likely. When these ranges are considered, the average thickness of the secondary Martian crust is 27–37 km with a possible range of 0–71 km; however, the lower and upper limits of this range are unreasonable when the young crystallization ages of the SNC meteorites [Nyquist *et al.*, 2001] and the budget of heat producing elements in the mantle after planetary differentiation [McLennan, 2001, 2003] are considered, respectively.

¹Department of Geosciences, Stony Brook University, Stony Brook, New York, USA.

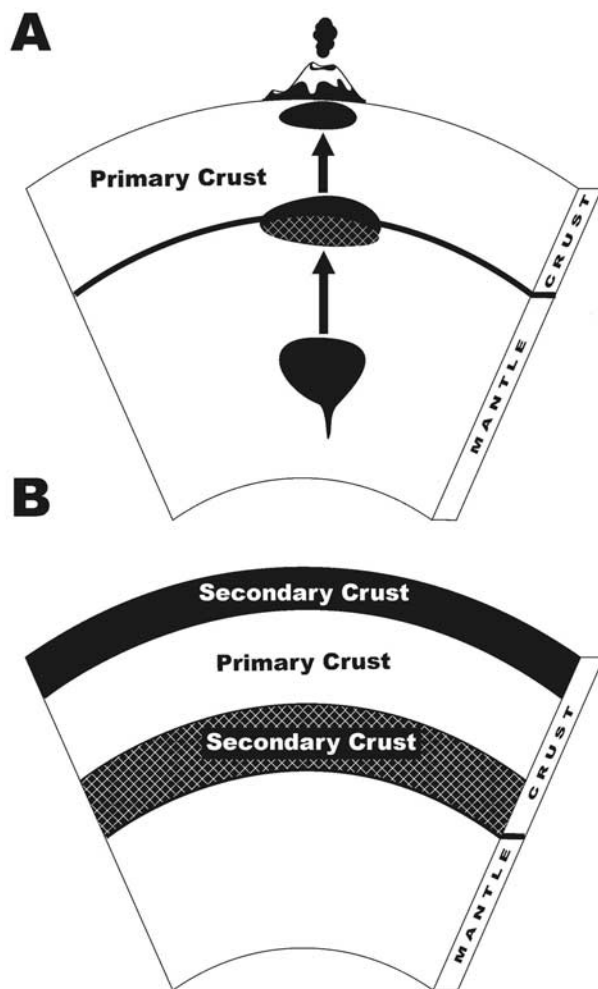


Figure 1. (A) Schematic illustrating the process of single-stage fractional crystallization at the base of a thick crust in which liquids residual to fractionation ascend to the surface or subsurface. (B) The residual liquids become part of the secondary, post-magma-ocean upper crust, while the cumulus minerals left at depth contribute to the formation of a deep, dense secondary lower crust.

[4] Given that the Martian crust is composed of at least some post-magma ocean igneous lithologies, the possibility exists for a compositionally diverse crust. In fact, some lithologic diversity has been observed on the Martian surface. *Bandfield et al.* [2004] and *Christensen et al.* [2005] have shown using various infrared instruments (Thermal Emission Imaging System [THEMIS] and Thermal Emission Spectrometer [TES]) that silica-rich lithologies exist on the Martian surface that deviate greatly from the basaltic materials that have been analyzed by the MER rovers [*Clark et al.*, 2005; *Gellert et al.*, 2006]. In order to understand the extent of crustal diversity on Mars, comparison with terrestrial magmatic processes that give rise to such diversity on Earth can be very useful. Because of both the thick crust and the lack of evidence for plate tectonics [*Breuer and Spohn*, 2003 and references therein], cratonic

intraplate magmatism is a good terrestrial analogue for the processes dictating lithologic diversity on the Martian surface.

[5] It has been accepted for many years that igneous compositional diversity on Earth can arise by fractionation of mantle-derived magmas at depth (within or at the base of the crust) and subsequent ascent of residual liquids into the upper crust at various stages of fractionation [e.g., *Albarede et al.*, 1997; *Cox*, 1972; *MacDonald*, 1968; *Naumann and Geist*, 1999; *Nekvasil et al.*, 2004; *Whitaker et al.*, 2007; *Wright*, 1970]. In intraplate regions of thick crust on Earth, fractionation of tholeiite at the base of the crust and ascent of residual liquids has been called upon to produce lithologies as diverse as Fe-Ti-P-enriched ferrobasalts and anorthosites (along with their associated ferrodiorites, syenites, and potassic granites) [*Scoates et al.*, 1999; *Thompson*, 1975; *Whitaker et al.*, 2007], sodic silica-saturated alkalic suites that produce hawaiite, tristanite, trachyte, and sodic rhyolite [*Nekvasil et al.*, 2004], and nepheline (*ne*) normative hawaiites and phonolites [*Filiberto and Nekvasil*, 2003]. The nature of the magmatic diversity arising in this manner likely varies not only with bulk silicate composition but also with differing amounts of bulk water in the parental magma. *Whitaker et al.* [2005] have shown that terrestrial tholeiite having a bulk water content $< \sim 0.4$ wt% fractionating at 9.3 kbar, will give rise to a silica-depletion trend in the residual liquids, resulting in Fe-rich and Si-poor evolved magmas. In contrast, when bulk water contents were above this value, a silica-enrichment trend was observed in the residual liquids. While fractional crystallization is accepted as a magmatic process on Earth, there is little consensus regarding how important a role fractional crystallization has played for Martian magmas [*Christensen et al.*, 2005; *McSween and Harvey*, 1993; *McSween et al.*, 2006a; *Nekvasil et al.*, 2007; *Rogers and Christensen*, 2007; *Taylor et al.*, 2006; *Whitaker et al.*, 2005].

Table 1. Published Humphrey Compositions and Synthetic Compositions Used in This Study

Oxide	Hbrush ^a	HRAT 1 ^a	HRAT 2 ^a	Hsynth Dry ^b	Hsynth Wet ^b
SiO ₂	45.9	46.3	45.9	47.7	45.8
TiO ₂	0.54	0.58	0.55	0.53	0.54
Al ₂ O ₃	11.2	10.8	10.7	10.9	10.4
Cr ₂ O ₃	0.60	0.68	0.60	0.67	0.63
FeO	17.9	18.6	18.8	17.9	18.1
MgO	8.82	9.49	10.4	9.57	9.19
CaO	7.76	8.19	7.84	8.09	7.77
Na ₂ O	3.00	2.80	2.50	2.72	2.70
K ₂ O	0.18	0.13	0.10	0.16	0.14
MnO	0.39	0.41	0.41	0.38	0.41
P ₂ O ₅	0.62	0.57	0.56	0.61	0.62
F	n.d.	n.d.	n.d.	0.56	0.55
Cl	0.62	0.57	0.56	0.15	0.21
-O = F + Cl	0.11	0.07	0.06	0.27	0.28
Total	97.4	99.1	98.9	99.7	96.8
mg# ^c	0.51	0.52	0.54	0.53	0.52
H ₂ O in synthetic glass (wt%)				0.07 ^d	1.67 ^d

^a*Gellert et al.* [2006].

^bSynthetic composition used for this study.

^cmg# = Molar Mg/(Mg + Fe²⁺) assuming an Fe²⁺/Fe_{tot} ratio of 0.85.

^dMeasured by FTIR (not included in total).

Table 2. Mineral Phase Compositions From Experiments on Hsynth Dry (0.07 wt% Bulk H₂O^a) at 9.3 kbar

Phase	Cr-Spinel					Olivine	
	Experiment	3.025	3.008	3.009	3.011		3.010
Temperature (°C)		1250	1200	1150	1120	1100	1250
SiO ₂		0.00	0.00	0.00	0.00	0.00	37.0
TiO ₂		0.77	0.94	1.91	2.12	3.23	0.02
Al ₂ O ₃		19.8	22.3	20.5	27.6	20.2	0.07
Cr ₂ O ₃		45.1	44.00	40.4	31.7	35.1	0.60
FeO		23.1	24.7	28.6	31.8	32.7	25.9
MnO		0.15	0.14	0.22	0.17	0.21	0.29
MgO		8.42	7.59	5.25	5.09	4.19	34.3
CaO		0.11	0.25	0.23	0.16	0.29	0.27
Na ₂ O		0.05	0.03	0.05	0.03	0.01	0.03
K ₂ O		0.01	0.01	0.03	0.03	0.01	0.00
P ₂ O ₅		0.01	0.02	0.02	0.04	0.01	0.27
Total		98.6	100.0	97.2	98.7	96.0	98.7
Phase Comp. (mol%)		U ₁ Mt ₁ Cr ₅₈ Hy ₃₈	U ₂ Mt ₀ Cr ₅₆ Hy ₄₂	U ₅ Mt ₁ Cr ₅₄ Hy ₄₁	U ₅ Mt ₂ Cr ₄₀ Hy ₅₂	U ₈ Mt ₄ Cr ₄₇ Hy ₄₁	Fo ₇₀ (La _{0.39})
Phase	Olivine				Pigeonite		
Experiment		3.008	3.009	3.011	3.010	3.008	3.009
Temperature (°C)		1200	1150	1120	1100	1200	1150
SiO ₂		36.4	34.3	34.2	33.9	50.4	48.8
TiO ₂		0.03	0.05	0.05	0.06	0.22	0.39
Al ₂ O ₃		0.06	0.08	0.05	0.06	3.68	5.20
Cr ₂ O ₃		0.29	0.19	0.12	0.19	1.63	0.76
FeO		29.9	39.2	43.8	42.7	16.1	17.9
MnO		0.50	0.47	0.41	0.41	0.51	0.48
MgO		31.4	24.7	20.9	21.0	19.9	15.4
CaO		0.42	0.37	0.41	0.44	5.44	8.45
Na ₂ O		0.03	0.08	0.05	0.03	0.23	0.54
K ₂ O		0.01	0.03	0.01	0.00	0.00	0.03
P ₂ O ₅		0.09	0.11	0.22	0.16	0.11	0.14
Total		99.1	99.6	100.2	98.9	98.2	98.1
Phase Comp. (mol%)		Fo ₆₅ (La _{0.62})	Fo ₅₃ (La _{0.56})	Fo ₄₆ (La _{0.64})	Fo ₄₆ (La _{0.71})	En ₅₉ Wo ₁₄	En ₄₇ Wo ₂₃
Phase	Pigeonite		Plagioclase		Augite		
Experiment		3.011	3.010	3.009	3.011	3.010	3.010
Temperature (°C)		1120	1100	1150	1120	1100	1100
SiO ₂		49.1	49.7	57.3	57.4	59.3	45.9
TiO ₂		0.48	0.47	0.04	0.05	0.05	0.87
Al ₂ O ₃		5.51	2.58	26.5	25.6	25.9	8.06
Cr ₂ O ₃		1.13	0.84	0.05	0.02	0.00	2.10
FeO		19.2	20.1	0.43	0.67	0.60	14.1
MnO		0.31	0.34	0.03	0.01	0.01	0.27
MgO		13.6	13.9	0.09	0.06	0.08	10.4
CaO		9.55	9.95	8.95	8.06	7.75	15.0
Na ₂ O		0.55	0.33	6.44 ^b	6.75 ^b (6.38)	7.20 ^b (6.95)	0.58
K ₂ O		0.01	0.00	0.16	0.22	0.24	0.00
P ₂ O ₅		0.26	0.13	0.21	0.16	0.15	0.55
Total		99.7	98.3	100.2	99.0	101.3	97.8
Phase Comp. (mol%)		En ₄₂ Wo ₂₅	En ₄₂ Wo ₂₅	An ₄₂ (Or ₁)	An ₃₈ (Or ₁)	An ₃₆ (Or ₁)	En ₄₄ Wo ₂₃

^aMeasured by FTIR.^bValue corrected for Na-loss; measured value listed parenthetically.

[6] Fractional crystallization taking place at the base of or within the lower crust has major implications for the development of igneous stratigraphy and retention of such stratigraphy in the absence of subduction-related tectonics. Figure 1 shows schematically the crustal stratigraphy that would arise from fractionation of a magma at the base of the crust followed by emplacement of the residual melt at shallow levels or eruption onto the surface. However, what is the extent of the lithologic diversity that can be produced solely by this process, and what are the compositional differences and volume relationships between the ascending residual magmas and the crystalline phases accumulating at the base of the crust?

[7] The goal of this work is to provide constraints on the compositions and volumetric abundances of evolved magmas that could have contributed to the current Martian surface upon crystallization of a “primary” mantle-derived magma at the base of a thick Martian crust (chosen as ~70 km depth or 9.3 kbar pressure) by experimentally determining the nature of the residual liquids and fractionating mineral assemblages for both “wet” (1.67 wt%) and “dry” (0.07 wt%) compositions. The composition chosen for this study is that of the rock Humphrey, which is one of the Adirondack-class basalts analyzed by the MER rover Spirit in Gusev Crater, Mars [Squyres *et al.*, 2006]. The Adirondack-class basalts are picobasalts that are believed to represent “near-primary”

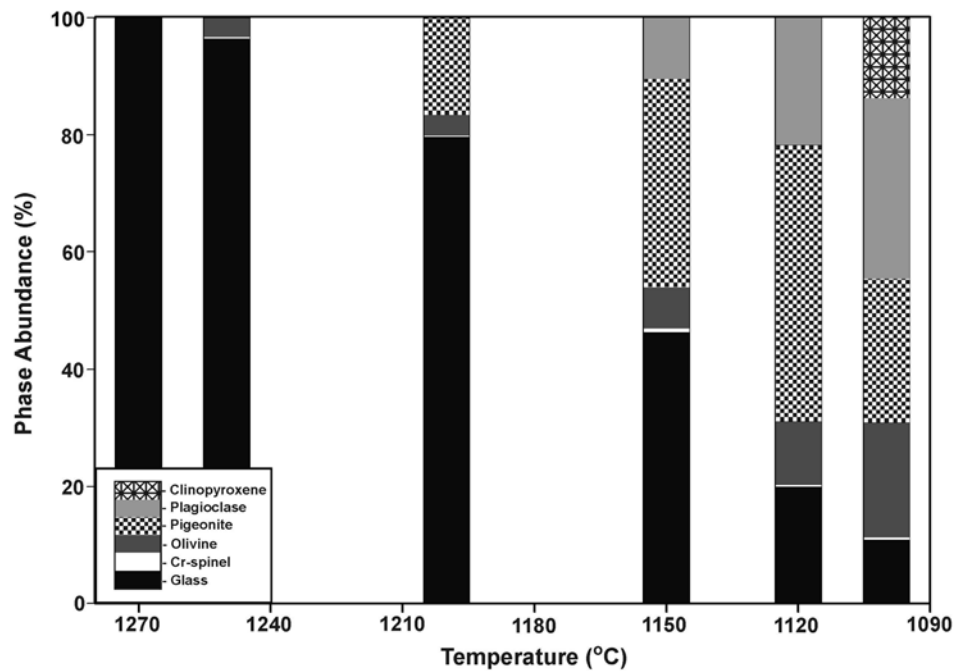


Figure 2. Abundances of phases formed in crystallization experiments on Humphrey composition liquid with 0.07 wt% bulk water at 9.3 kbar. Abundances were calculated using the least squares mass balance routine of the IgPet software suite [Carr, 2002].

Martian melts [Monders *et al.*, 2007]. Texturally, Humphrey is a fine-grained vesicular basalt with up-to 25% megacrystic olivine [McSween *et al.*, 2006b]. Some debate exists as to whether or not the megacrystic olivine represents grains crystallized in situ or grains that were accumulated (if the grains were accumulated, then the reported composition for Humphrey would be displaced from a liquid composition); however, for the purposes of this study, it is assumed that Humphrey is representative of a liquid composition (after the views of McSween *et al.* [2006b], Monders *et al.* [2007], and Filiberto [2008]). Because the magmatic volatiles fluorine and chlorine are also likely constituents in Martian basalts [i.e., Gellert *et al.*, 2006; Greenwood, 2005; McCubbin and Nekvasil, 2008], some fluorine and chlorine were added to the Humphrey composition so that the effect of water could be understood in the presence of such volatiles.

2. Analytical/Experimental Methods

2.1. Strategy

[8] Crystallization experiments in which the starting material was melted before cooling to the temperature of interest were conducted at a range of temperatures at a pressure of 9.3 kbar to assess the compositions of the minerals and melts at various potential stages of melt separation. Relative abundances of all phases at each potential stage of liquid separation were computed by mass balance using analyses of residual liquids (i.e., the quenched glass of any given experiment) and all crystalline phases. Starting water contents of 0.07 wt% and 1.67 wt% were chosen in order to assess the effect of bulk water contents on liquid evolution.

2.2. Experimental Methods

2.2.1. Starting Materials

[9] A mix was designed based on the Humphrey Rat 1 composition reported by Gellert *et al.* [2006] (reported in Table 1) but with 1500 ppm chlorine and 5000 ppm fluorine added. The mix was created by first accurately weighing oxide, Fe⁰, CaF₂, and NaCl powders in the proportions needed for obtaining the desired composition. Next, the powders were mechanically mixed sequentially by volume in an automatic agate mortar/pestle grinder for a total of 3.5 h. The Fe³⁺/ΣFe value in the mixture was 0.16. Because NaCl is soluble in ethanol, it was added to the mix subsequent to drying. The composition of this

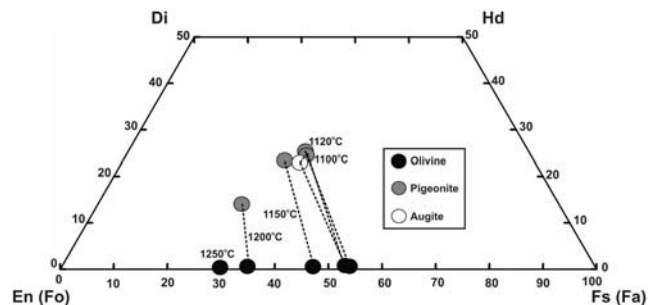


Figure 3. Projected compositions of ferromagnesian phases crystallized from experiments on Humphrey with 0.07 wt% bulk water. Phases plotted using the projection scheme of the program QUILF [Andersen *et al.*, 1993]. Dashed lines connect phases co-existing at the indicated temperatures. See text for explanation of apparent inconsistencies between augite and pigeonite compositions.

Table 3. Residual Liquid Compositions From Experiments on Hsynth Dry (0.07 wt% Bulk H₂O^a) at 9.3 kbar

Experiment (No.) Mode (wt%)	3.025 Gl 96.5, Ol 3.2, Sp 0.3	3.008 Gl 79.7, Ol 3.5, Sp 0.2, Pig 16.6	3.009 Gl 46.3, Ol 7.0, Sp 0.7, Pig 35.6, Pl 10.4,	3.011 Gl 20.0, Ol 10.8, Sp 0.4, Pig 47.1, Pl 21.7	3.010 Gl 10.9, Ol 19.7, Sp 0.4, Pig 24.4, Pl 30.9, Cpx 13.7
Temperature (°C)	1250	1200	1150	1120	1100
SiO ₂	47.5	46.2	45.2	42.8	40.2
TiO ₂	0.57	0.65	0.90	1.38	1.62
Al ₂ O ₃	11.3	13.2	12.9	12.7	10.6
Cr ₂ O ₃	0.46	0.26	0.15	0.10	0.08
FeO	17.6	17.2	17.6	19.3	21.4
MnO	0.21	0.41	0.36	0.40	0.27
MgO	8.53	6.67	4.75	4.40	4.10
CaO	8.15	9.21	8.58	8.91	10.5
Na ₂ O ^b	2.76	n.c.	n.c.	4.90	n.c.
Na ₂ O	2.38	3.16	3.94	3.69	3.69
K ₂ O	0.17 ^c	0.21 ^c	0.31	0.48	0.54
P ₂ O ₅	0.64	0.89	1.17	2.12	2.46
F ^c	0.58	0.70	1.21	2.80	5.14
Cl ^c	0.16	0.19	0.32	0.75	1.38
–O = F + Cl	0.28	0.34	0.58	1.35	2.48
Total	98.4	98.6	96.8	99.7	99.5
mg# ^d	0.50	0.44	0.36	0.32	0.29
H ₂ O in Glass (wt%) ^b	0.07	0.09	0.15	0.35	0.64
Crystallinity (wt%)	3.5	20.2	53.6	80.0	89.1
S.S.R.	0.13	0.20	0.01	0.02	0.06

^aMeasured by FTIR.^bValue corrected for Na-loss.^cCalculated based on degree of crystallinity assuming component increases incompatibly (H₂O value not included in total).^dmg# = Molar Mg/(Mg + Fe²⁺) assuming an Fe²⁺/Fe_{tot} ratio of 0.85.

synthetic Humphrey mixture (Hsynth Dry) is reported in Table 1.

2.2.2. Piston-Cylinder Experiments

[10] For each experiment conducted under “dry” conditions, the Humphrey powder was loaded into a graphite capsule and dried under vacuum at 800°C in a tube furnace in the presence of a Fe^o oxygen getter for 20 min to remove structurally bound and adsorbed water. Subsequent to drying, the capsule was loaded into a BaCO₃ cell using the same cell assembly reported by *Whitaker et al.* [2007]. The assembled cell was then placed within a 1/2 inch [1.27 cm] piston-cylinder apparatus (using the piston-out method) and pressurized immediately to prevent water adsorption. Next the temperature was raised to a melting temperature of 1372°C. After melting for 2.5 h, the temperature was rapidly dropped to the desired crystallization temperature and left to crystallize for a minimum of 2.5 days. The temperature of each experiment was both controlled and monitored by a Pt–Pt₉₀Rh₁₀ thermocouple. At the end of each experiment, the run was rapidly quenched isobarically.

[11] For experiments run under hydrous conditions, synthesis of a hydrous glass was required. This was done by first loading water into a graphite-lined Pt-capsule before adding the synthetic Humphrey powder. Once the powder was loaded, the capsule’s lid was welded on, and the capsule was inserted into a talc cell. The talc cell was then placed within a 3/4 inch [1.90 cm] piston-cylinder apparatus and pressurized to 9.3 kbar. The temperature was then raised to 1330°C and left to melt for 2.5 h before rapidly quenching isobarically. The water content of the resulting glass was determined by micro-FTIR to be 3.31 wt%. This hydrous glass was then mixed with dried synthetic Humphrey powder in order to obtain the desired

starting water content of 1.67 wt%. This mixture (Hsynth Wet, reported in Table 1) was used for all hydrous experiments reported for this work.

[12] Experiments using the hydrous Humphrey powder were conducted in the same manner as the “dry” experiments with two exceptions. Instead of drying at 800°C, the loaded capsule was dried in a drying oven under vacuum at 130–150°C for 90 min to remove adsorbed water only. Second, the melting temperature for the “wet” experiments was 1330°C.

[13] Since the experiments were performed in graphite capsules, the fO₂ was partially controlled by the graphite–CO–CO₂ (GCO) buffer. However, because no direct evidence was observed for the presence of a fluid, the GCO buffer provides only an upper limit to fO₂ [*Eugster and Skippen*, 1967]. *Whitaker et al.* [2007] used the same experimental technique and reported that the fO₂ at 9.3 kbar typically ranged from 1.5 to 2.5 log units below the fayalite-magnetite-quartz (FMQ) buffer (using the QUILF routine of *Andersen et al.* [1993]). None of our phase assemblages were appropriate for using QUILF to estimate fO₂, but we assume that it was similar to that reported by *Whitaker et al.* [2007].

2.3. Analytical Methods

2.3.1. EPMA Analysis

[14] Electron probe microanalysis (EPMA) (exclusive of fluorine in glass and amphibole) was performed using a Cameca Camebax electron microprobe (EMP) equipped with four wavelength dispersive spectrometers. An accelerating voltage of 15 kV and a nominal beam current of 10 nA were used during analysis. For Na-bearing phases, the largest possible raster size was used to minimize unknown analytical problems that occur during highly focused elec-

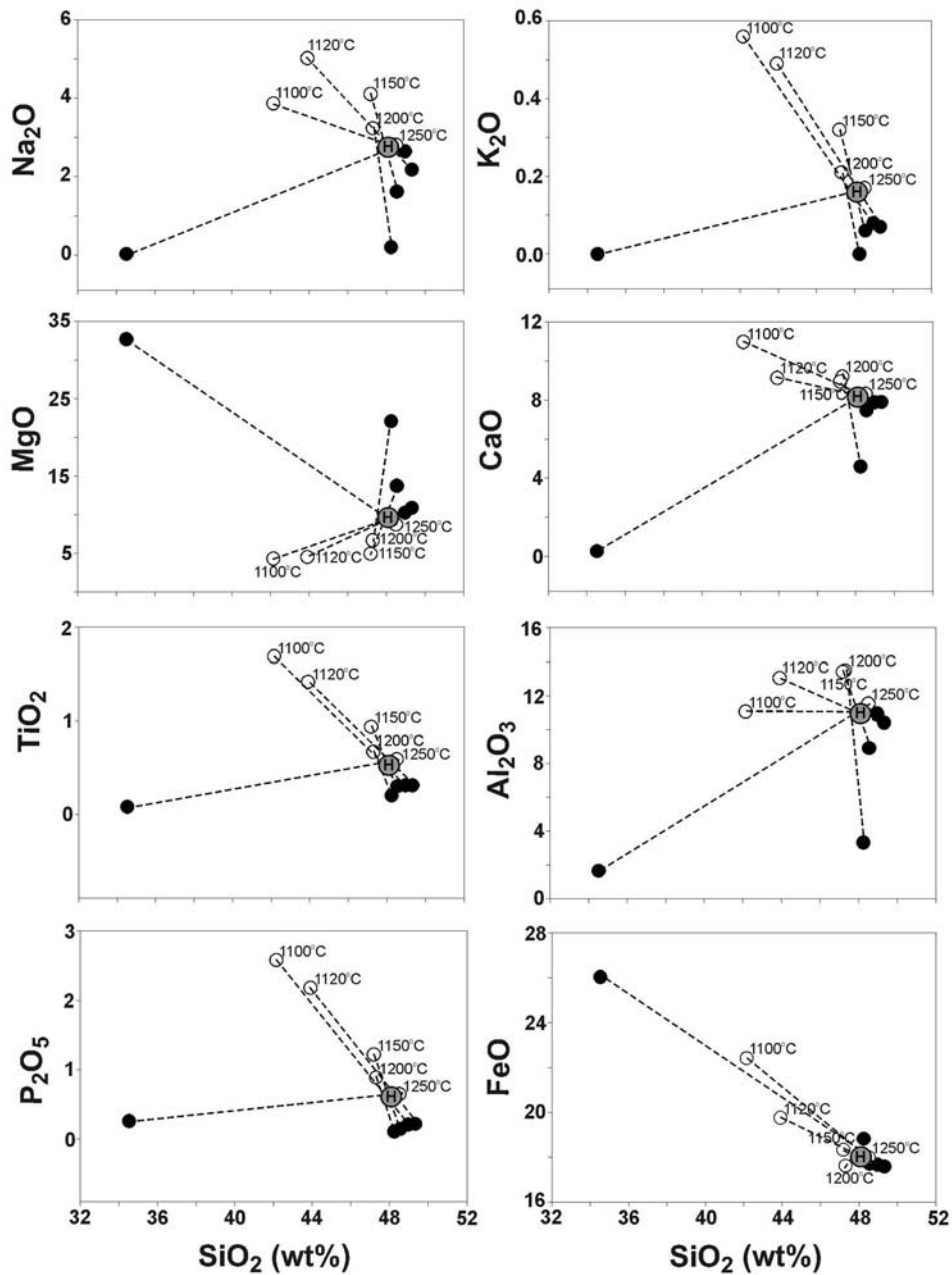


Figure 4. Harker-variation diagram for (open circles) residual liquids and (black circles) bulk solids from experiments on Humphrey (H) with 0.07 wt% bulk water at 9.3 kbar. Coexisting phases at each temperature are connected by dashed lines.

tron beam analysis on such matrices. However, this alone did not prevent apparent Na-loss. Adopting the correction technique of *McCubbin and Nekvasil* [2008], Na was added back into the analysis such that normative corundum was no longer present for any Na-bearing phase. The IgPet Program Suite [Carr, 2002] was used to conduct mass-balance calculations using a least-squares routine. This was done to verify that no phase was overlooked during EPMA analysis, and to quantitatively estimate phase abundances. The computed phase abundances were used to calculate the bulk solid composition of the fractionating mineral assemblage at each temperature.

[15] EMP analysis of the fluorine-bearing phases glass and amphibole were conducted with a Cameca SX100 microprobe at the American Museum of Natural History. Major element analyses were conducted with a 2 nA beam current, 15 kV accelerating voltage, and 10 μm beam diameter for Na. All other elements were measured using 10 nA and 15 kV with a 10 μm beam diameter.

2.3.2. Micro-FTIR Spectroscopy

[16] Quantitative infrared spectroscopic measurements were conducted on experimental glass products at room-temperature in transmittance mode with a Thermo Nicolet 20SXB FTIR spectrometer attached to a Spectra Tech IR

Table 4. Computed^a Bulk Residual Solid Compositions From Experiments on Hsynth Dry (0.07 wt% Bulk H₂O^b) at 9.3 kbar

Experiment (No.)	3.025	3.008	3.009	3.011	3.010
Temperature (°C)	1250	1200	1150	1120	1100
SiO ₂	34.5	48.2	48.5	49.3	49.0
TiO ₂	0.08	0.20	0.30	0.31	0.31
Al ₂ O ₃	1.65	3.32	8.91	10.4	11.0
Cr ₂ O ₃	4.17	1.89	1.09	0.85	0.75
FeO	26.0	18.8	17.7	17.6	17.7
MnO	0.28	0.51	0.39	0.24	0.23
MgO	32.7	22.1	13.7	10.9	10.3
CaO	0.26	4.60	7.48	7.91	7.89
Na ₂ O	0.03	0.20	1.62 ^c	2.18 ^c	2.65 ^c
K ₂ O	0.00	0.00	0.06	0.07	0.08
P ₂ O ₅	0.26	0.11	0.15	0.22	0.21
Total	99.9	99.9	99.9	100.0	100.1
mg# ^d	0.73	0.71	0.62	0.56	0.55

^aComputed from phase abundances.^bMeasured by FTIR.^cValue calculated from plagioclase that was corrected for Na-loss.^dmg# = Molar Mg/(Mg + Fe²⁺) assuming an Fe²⁺/Fe_{Total} ratio of 0.85.

Plan microscope located in the Department of Earth and Planetary Sciences at the American Museum of Natural History. Both the spectrometer and the IR objective were purged with dry nitrogen gas at a rate of 15 l/min. Transmittance IR spectra were collected from doubly polished wafers of the run products over the mid-IR (1400–4000 cm⁻¹) to near-IR regions (3700–6500 cm⁻¹) using a KBr beam splitter, MCT/A detector, and globar source. Total dissolved water concentrations were determined for each glass from the intensity of the broad band at 3570 cm⁻¹ after the calculation scheme of *Mandeville et al.* [2002]. Approximately 1024 scans were performed for each IR spectrum acquired at a resolution of 4 cm⁻¹. All spots were first assessed optically to ensure that only glass was being measured during each analysis.

3. Experimental Results

3.1. “Dry” Experiments

[17] Experiments on the synthetic Humphrey mix under “dry” conditions at 9.3 kbar were conducted over the temperature interval 1270–1100°C. The run products of the experiments contained variable amounts of mineral phases and glass. Micro-FTIR analysis of residual glass indicates a starting water content of 0.07 wt%.

3.1.1. Mineral Phases

[18] Compositions of mineral phases that formed during “dry” crystallization of Humphrey (Hsynth Dry) are presented in Table 2. Figure 2 shows the computed phase abundances from the experimental run products. Olivine and Cr-spinel are on the liquidus, and the next phase to appear is pigeonite at 1200°C, followed by plagioclase at 1150°C, and eventually augite at 1100°C. Once each phase enters the assemblage, it persists throughout the entire range of investigated temperatures.

[19] Figure 3 shows olivine and pyroxene compositions projected into the pyroxene quadrilateral through QUILF [*Andersen et al.*, 1993]. Wollastonite components (Wo) of pigeonite range from Wo₁₄ to Wo₂₅, while the single augite has an apparent Wo content of 23 mol%. The higher Wo-content of some pigeonite compositions compared with the augite is an

artifact of the QUILF projection scheme, arising from over-correction of Wo in pigeonite and undercorrection in augite resulting from non-quadrilateral components in those phases. Although the plotted compositions look unusual, they have very little thermodynamic consequence because they lie near the crest of the augite solvus [personal communication from DHL]. Olivine ranges in composition from Fo₇₀ to Fo₄₆.

3.1.2. Liquid Evolution

[20] For the “dry” Humphrey composition, the liquidus temperature at 9.3 kbar is between 1250°C and 1270°C; the solidus temperature is below 1100°C (Figure 2). Table 3 and Figure 4 illustrate the compositional evolution of residual liquids (i.e., glass product analyzed for each run and re-cast on a volatile-free basis in Figure 4) and bulk solids (Table 4) along the “dry” crystallization path with decreasing temperature. As seen in Figure 3, the residual liquids exhibit a silica-depletion trend having strong K-, Ti-, P-, and Fe-enrichment with dropping temperature. Both Al and Na show initial enrichment but decrease toward starting values once plagioclase becomes stable. Ca remains relatively constant for much of the temperature interval investigated with the exception of the 1100°C experiment in which Ca increases by ~20%. Mg follows a depletion trend throughout the investigated temperature interval. The bulk liquid starts out hypersthene (*hy*)-normative but becomes nepheline (*ne*)-normative between 1200°C and 1150°C. The liquid remains *ne*-normative as crystallization proceeds.

[21] The magmatic volatiles fluorine and chlorine increase incompatibly throughout the temperature interval investigated. Chlorine abundance was likely well below that needed to form either an immiscible chloride melt or a Cl-bearing fluid. Fluorine contents approached high values and loss of an F-rich fluid phase (while unlikely) could have occurred; therefore, the computed fluorine contents presented in Table 3 are upper limits.

3.2. “Wet” Experiments

[22] Experiments on the synthetic Humphrey mix under “wet” conditions at 9.3 kbar were conducted over the temperature interval 1250–980°C. The run products of the experiments contained variable amounts of mineral phases and glass. Micro-FTIR analysis of residual glass indicates a bulk (initial) water content of 1.67 wt%.

3.2.1. Mineral Phases

[23] Compositions of mineral phases that formed during “wet” crystallization of Humphrey (Hsynth Wet) are presented in Tables 5 and 6. Figure 5 shows the computed phase abundances from these experiments. While Cr-spinel appears to be the liquidus phase, it is likely metastable as it formed during hydrous glass synthesis and, because of its refractory nature, did not dissolve during the experiments. Therefore the liquidus is likely represented by the appearance of olivine at 1200°C (at which point Cr-spinel may also be stable). Orthopyroxene then appears at 1150°C, and at 1100°C orthopyroxene is replaced by pigeonite. Augite enters the assemblage at 1050°C, followed by amphibole at 1030°C. At 1000°C, augite is no longer present, and plagioclase and apatite appear. At 980°C olivine is no longer part of the assemblage.

[24] Figure 6 shows olivine and pyroxene compositions projected into the pyroxene quadrilateral through QUILF [*Andersen et al.*, 1993]. Amphibole is also projected into the

Table 5. Compositions of Volatile-Free Minerals From Experiments on Hsynth Wet (1.67 wt% Bulk H₂O^b) at 9.3 kbar

Phase	Cr-Spinel										
	Experiment Temperature (°C)	3.026 1250	3.029 1200	3.022 1150	3.023 1100	3.027 1050	3.028 1030	3.030 1000	3.028 980	3.032 980	
SiO ₂	0.00	0.00	0.00	0.00	0.00	0.00	0.00	0.00	0.00	0.00	
TiO ₂	0.45	0.41	1.19	1.33	1.33	1.03	0.48	0.41	0.40	0.40	
Al ₂ O ₃	9.14	9.85	16.4	17.4	17.4	15.3	10.1	9.02	8.78	8.78	
Cr ₂ O ₃	56.0	53.3	43.2	40.4	40.4	41.8	52.8	51.5	51.7	51.7	
FeO	25.6	26.3	29.7	31.9	31.9	31.4	30.7	31.5	30.8	30.8	
MnO	0.19	0.18	0.20	0.20	0.20	0.23	0.17	0.32	0.38	0.38	
MgO	7.02	6.90	6.37	5.63	5.63	4.35	3.35	3.15	2.76	2.76	
CaO	0.25	0.21	0.20	0.28	0.28	0.29	0.21	0.23	0.12	0.12	
Na ₂ O	0.04	0.03	0.00	0.04	0.04	0.04	0.02	0.02	0.03	0.03	
K ₂ O	0.00	0.01	0.01	0.00	0.00	0.00	0.00	0.00	0.01	0.01	
P ₂ O ₅	0.02	0.05	0.01	0.02	0.00	0.03	0.00	0.00	0.02	0.02	
Total	98.7	97.3	97.3	97.2	97.2	94.5	97.8	96.2	95.0	95.0	
Phase Comp. (mol%)	U ₁₁ Mt ₄ Cr ₇₆ Hy ₁₈	U ₁₁ Mt ₁₆ Cr ₇₃ Hy ₂₀	U ₁₃ Mt ₁₇ Cr ₅₈ Hy ₅₃	U ₁₃ Mt ₈ Cr ₅₄ Hy ₃₅	U ₁₃ Mt ₈ Cr ₅₄ Hy ₃₅	U ₁₃ Mt ₇ Cr ₅₈ Hy ₃₂	U ₁₁ Mt ₄ Cr ₇₄ Hy ₂₁	U ₁₁ Mt ₈ Cr ₇₄ Hy ₁₉	U ₁₁ Mt ₅ Cr ₇₅ Hy ₁₉	U ₁₁ Mt ₅ Cr ₇₅ Hy ₁₉	
Phase	Olivine					Orthopyroxene					Pigeonite
Experiment Temperature (°C)	3.029 1200	3.022 1150	3.023 1100	3.027 1050	3.027 1050	3.028 1030	3.030 1000	3.022 1150	3.028 1100	3.023 1100	
SiO ₂	37.6	37.5	36.4	35.1	35.1	34.9	33.3	52.9	52.0	52.0	
TiO ₂	0.02	0.01	0.02	0.00	0.00	0.01	0.04	0.10	0.12	0.12	
Al ₂ O ₃	0.05	0.02	0.03	0.01	0.01	0.01	0.02	1.93	2.37	2.37	
Cr ₂ O ₃	0.14	0.09	0.12	0.09	0.09	0.06	0.02	0.79	0.65	0.65	
FeO	26.4	30.5	34.0	38.3	38.3	42.9	46.8	18.0	18.3	18.3	
MnO	0.30	0.52	0.31	0.40	0.40	0.40	0.40	0.28	0.37	0.37	
MgO	35.6	32.6	29.0	25.4	25.4	21.6	18.6	23.6	19.7	19.7	
CaO	0.21	0.19	0.31	0.22	0.22	0.24	0.21	1.86	6.33	6.33	
Na ₂ O	0.00	0.00	0.02	0.01	0.01	0.02	0.02	0.07	0.20	0.20	
K ₂ O	0.01	0.00	0.01	0.00	0.00	0.00	0.02	0.00	0.00	0.00	
P ₂ O ₅	0.05	0.05	0.06	0.08	0.08	0.19	0.10	0.11	0.11	0.11	
Total	100.4	101.5	100.3	99.6	99.6	100.3	99.5	99.6	100.2	100.2	
Phase Comp. (mol%)	Fe ₇₀ (La _{0.30})	Fe ₆₅ (La _{0.28})	Fe ₆₀ (La _{0.46})	Fe ₅₄ (La _{0.34})	Fe ₅₄ (La _{0.34})	Fe ₄₇ (La _{0.38})	Fe ₄₆ (La _{0.71})	En ₆₇ Wo ₄	En ₅₆ Wo ₁₆	En ₅₆ Wo ₁₆	

Table 5. (continued)

Phase Experiment Temperature (°C)	Pigeonite			Augite			Plagioclase		
	3.027 1050	3.028 1030	3.032 980	3.027 1050	3.028 1030	3.030 1000	3.027 1050	3.028 1030	3.030 1000
SiO ₂	51.1	50.7	49.5	50.1	50.5	56.6	50.1	50.5	56.6
TiO ₂	0.20	0.14	0.05	0.25	0.29	0.02	0.25	0.29	0.02
Al ₂ O ₃	2.85	2.82	2.63	3.32	3.82	27.9	3.32	3.82	27.9
Cr ₂ O ₃	0.58	0.34	0.31	0.82	0.63	0.00	0.82	0.63	0.00
FeO	20.3	24.7	26.7	14.1	16.9	0.85	14.1	16.9	0.85
MnO	0.38	0.45	0.64	0.27	0.29	0.01	0.27	0.29	0.01
MgO	18.5	14.2	13.6	14.2	13.9	0.05	14.2	13.9	0.05
CaO	5.12	6.85	5.22	15.6	13.1	9.65	15.6	13.1	9.65
Na ₂ O	0.16	0.26	0.21	0.38	0.40	5.99	0.38	0.40	5.99
K ₂ O	0.00	0.01	0.01	0.00	0.00	0.07	0.00	0.00	0.07
P ₂ O ₅	0.10	0.17	0.08	0.25	0.21	0.15	0.25	0.21	0.15
Total	99.3	99.7	99.0	99.3	100.0	101.3	99.3	100.0	101.3
Phase Comp. (mol%)	En ₅₄ Wo ₁₃	En ₄₂ Wo ₁₈	En ₄₂ Wo ₁₇	En ₄₇ Wo ₂₉	En ₄₆ Wo ₂₃	An ₄₆ (Or _{0.4})	En ₄₇ Wo ₂₉	En ₄₆ Wo ₂₃	An ₄₆ (Or _{0.4})

^aMeasured by FTIR.^bValue corrected for Na-loss; measured value is listed parenthetically.

quadrilateral by summing the ternary components (Ca, Mg, and Fe) and normalizing to one atom. Projection of amphibole into the quadrilateral was necessary for understanding the evolution of the ferromagnesian mineral phases since augite and olivine were likely reacting with melt to form amphibole. Wo-components of pigeonite range from Wo₁₃ to Wo₁₈, while the single orthopyroxene has Wo₄. Augite ranges from Wo₂₃ to Wo₂₉, and amphibole ranges from “Wo₂₁ to Wo₂₃.” Olivine ranges in composition from Fo₇₀ to Fo₄₆.

3.2.2. Liquid Evolution

[25] Compositions of residual liquids are presented in Table 7. As seen in Figure 5, the liquidus for this composition at 9.3 kbar is >1250°C; however, as discussed above, the apparent liquidus phase (Cr-spinel) is likely metastable, therefore the “true” (equilibrium) liquidus is likely closer to 1200°C. The solidus for this composition is <980°C. Figure 7 illustrates the compositional evolution of residual liquids (Table 7) and bulk solids (Table 8) along the “wet” crystallization path. The residual liquids follow a silica-enrichment trend, which is coupled with strong alkali- and Al-enrichment and strong Mg- and Fe-depletion. Both Ca and Ti increase initially, but both elements are depleted beyond the starting values once augite and amphibole stabilize respectively. The residual liquid starts out *hy*-normative and remains so throughout the investigated temperature interval.

[26] It has been our experience that once a water-rich fluid phase forms it escapes through the graphite capsule walls. The computed water values assume that formation and loss of a fluid phase did not occur; however, because fluid saturation may have been attained, the water contents presented in Table 7 are upper limits. Fluorine and chlorine increased incompatibly in the liquid until amphibole entered the assemblage at 1030°C; however, because chlorine is not easily incorporated into such amphiboles [Morrison, 1991], it continued to increase

Table 6. Compositions of Volatile-Bearing Minerals From Experiments on Hsynth Wet (1.67 wt% Bulk H₂O^a) at 9.3 kbar

Phase Experiment Temperature (°C)	Amphibole			Apatite	
	3.028 1030	3.030 1000	3.032 980	3.030 1000	3.032 980
SiO ₂	43.1	42.6	42.1	0.31	0.50
TiO ₂	1.23	1.18	1.09	<i>n.d.</i>	<i>n.d.</i>
Al ₂ O ₃	13.4	11.7	12.5	<i>n.d.</i>	<i>n.d.</i>
Cr ₂ O ₃	0.61	0.24	0.54	<i>n.d.</i>	<i>n.d.</i>
FeO	15.1	17.3	17.3	1.20	1.59
MnO	0.36	0.27	0.29	<i>n.d.</i>	<i>n.d.</i>
MgO	13.3	12.4	11.6	<i>n.d.</i>	<i>n.d.</i>
CaO	8.97	8.47	9.72	53.7	53.8
Na ₂ O	3.42	2.82	2.72	0.08	0.01
K ₂ O	0.08	0.14	0.11	<i>n.d.</i>	<i>n.d.</i>
P ₂ O ₅	0.02	0.03	0.06	41.6	41.1
F	1.45	1.42	1.10	2.85	3.13
Cl	0.06	0.07	0.08	0.40	0.59
-O = F + Cl	0.62	0.61	0.48	1.29	1.45
Total	100.5	98.0	98.8	98.0	99.3
Phase Comp. (mol%)	En ₄₇ Wo ₂₃	En ₄₄ Wo ₂₂	En ₄₁ Wo ₂₅	F _{0.77} Cl _{0.13}	F _{0.84} Cl _{0.19}
H ₂ O (wt%) ^b	1.40	1.36	1.44	0.18	0.00

^aMeasured by FTIR.^bCalculated assuming only F, Cl, and OH populate the volatile sites.

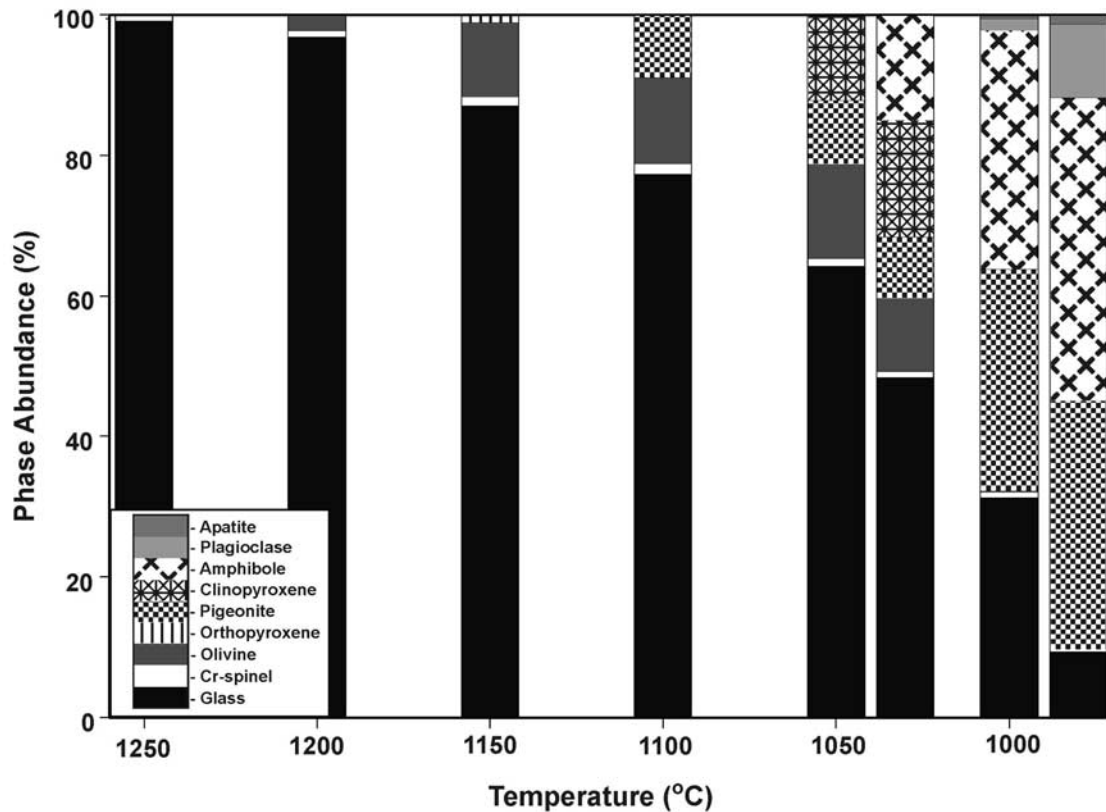


Figure 5. Abundances of phases formed in crystallization experiments on Humphrey composition liquid with 1.67 wt% bulk water at 9.3 kbar. Abundances were calculated using the least squares mass balance routine of the IgPet software suite [Carr, 2002].

nearly incompatibly until apatite entered the assemblage at 1000°C. Neither fluorine nor chlorine reached abundances in the melt that were consistent with fluid saturation, nor were their abundances sufficient to greatly enhance formation of a water-rich fluid [i.e., Webster *et al.*, 1999; Webster and Rebbert, 1998].

4. Discussion

4.1. Lithologic Diversity on the Martian Surface

[27] Although traditionally petrologists ascribe variations in rock chemistry to different mantle compositions and/or different degrees of partial melting, the experiments reported here illustrate the great range in compositional diversity of lavas on the Martian surface that could arise simply from a single stage of fractional crystallization of a Humphrey-like basaltic magma at the base of a thick crust. As has been observed for terrestrial rocks, the nature of the fractionation-induced compositional diversity is dependent upon differences in the bulk water content of the parental magma. Figure 8 shows that liquids evolving along the “dry” path change from basalt to basanite (an alkalic *ne-normative* basalt) and become progressively lower in silica with increasing degrees of fractionation. This contrasts greatly with liquids evolving along the “wet” path which progress from basalt to trachyandesite (an alkali-rich andesite according to the LeBas classification [LeBas *et al.*, 1986]). The opposing behavior of silica content with decreasing temperature in these two paths is perhaps

most readily seen via the magnesium number (mg#) (Figure 9). Once Humphrey-like magmas evolve to a mg# of 30, “dry” liquids would have silica contents close to 42 wt% while those starting from a melt with a water content of 1.67 wt% would have silica contents of 51 wt%.

[28] Importantly, evolution of “dry” magmas along the silica-depletion path is coupled with strong iron-enrichment

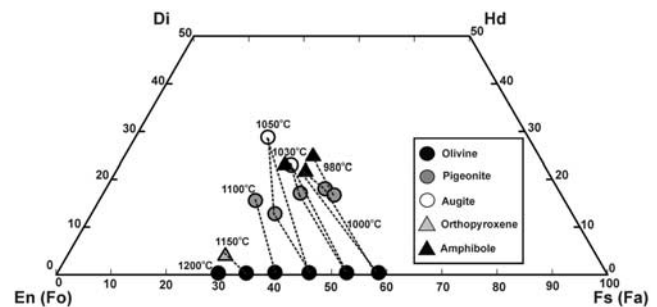


Figure 6. Projected compositions of ferromagnesian phases crystallized from experiments on Humphrey with 1.67 wt% bulk water at 9.3 kbar. Pyroxene and olivine compositions plotted using the projection scheme of the program QUILF [Andersen *et al.*, 1993]. For amphiboles, Ca + Mg + Fe were normalized to one atom. Dashed lines connect phases co-existing at the indicated temperatures.

Table 7. Residual Liquid Compositions From Experiments on Hsynth Wet (with 1.67 wt% Bulk H₂O^a) at 9.3 kbar

Experiment (No.) Mode (wt%)	3.026	3.029	3.022	3.023	3.027	3.028	3.030	3.032
	Gl 99.2, Sp 0.8	Gl 96.9, Sp 0.9, Ol 2.2	Gl 87.1, Sp 1.3, Ol 10.5, Opx 1.1	Gl 77.4, Sp 1.4, Ol 12.3, Pig 8.9	Gl 64.3, Sp 1.1, Ol 13.4, Pig 9.1, Cpx 12.1	Gl 48.6, Sp 0.8, Ol 11.0, Pig 7.2, Cpx 18.6, Amph 13.9	Gl 30.4, Sp 0.9, Ol 1.1, Pig 29.6, Amph 34.0, Plag 3.2, Ap 0.8	Gl 9.4, Sp 0.3, Pig 35.5, Amph 43.1, Plag 10.4, Ap 1.3
Temperature (°C)	1250	1200	1150	1100	1050	1030	1000	980
SiO ₂	46.3	45.0	47.6	48.5	47.8	48.7	49.4	53.3
TiO ₂	0.55	0.56	0.61	0.68	0.78	0.66	0.54	0.44
Al ₂ O ₃	10.6	10.6	11.8	13.1	15.1	15.5	15.4	15.8
Cr ₂ O ₃	0.22	0.10	0.06	0.04	0.02	0.04	0.05	0.05
FeO	18.2	17.4	16.6	15.7	14.5	13.9	14.3	12.0
MnO	0.27	0.25	0.22	0.20	0.19	0.15	0.19	0.26
MgO	9.24	8.40	6.41	5.19	4.02	3.09	2.39	1.25
CaO	7.98	7.79	8.81	9.13	8.49	7.62	7.02	6.13
Na ₂ O ^b	2.73	2.70	3.08	3.46	4.09	4.44	4.80	5.88
Na ₂ O	2.51	2.54	2.87	3.20	3.49	3.62	4.20	4.53
K ₂ O	0.15	0.14	0.17	0.20	0.22	0.26	0.40	0.61
P ₂ O ₅	0.62	0.65	0.71	0.81	0.92	1.03	1.10	0.79
F	0.55 ^c	0.57 ^c	0.63 ^c	0.71 ^c	0.86 ^c	0.80	0.81	0.52
Cl	0.21 ^c	0.22 ^c	0.24 ^c	0.27 ^c	0.33 ^c	0.44	0.74	1.22
–O = F + Cl	0.10	0.29	0.32	0.36	0.43	0.44	0.51	0.49
Total	97.3	94.1	96.6	97.6	96.9	96.2	96.6	97.8
mg# ^d	0.52	0.50	0.45	0.41	0.37	0.32	0.26	0.18
H ₂ O in Glass (wt%) ^c	1.68	1.72	1.92	2.15	2.60	3.26	4.85	10.0
Crystallinity (wt%)	0.8	3.1	12.9	22.6	35.7	51.5	68.6	90.6
S.S.R.	0.040	0.052	0.035	0.082	0.038	0.035	0.042	0.097

^aMeasured by FTIR.^bValue corrected for Na-loss.^cCalculated based on degree of crystallinity and composition of volatile-bearing minerals if present.^dmg# = Molar Mg/(Mg + Fe²⁺) assuming an Fe²⁺/Fe_{tot} ratio of 0.85.

of the residual liquids (Figure 10). By the time ~90% fractionation has taken place, the residual liquid would have over 22 wt% total iron. In contrast, the wetter starting material undergoing the same degree of fractionation would be depleted in total iron to a value below 12 wt%.

[29] The evolution of Humphrey along the “wet” or “dry” paths also has implications for the Al/Si ratio of the lavas representing liquids residual to deep fractionation. The Al/Si vs. Mg/Si ratios of the residual liquids for the “wet” Humphrey compositions evolve in a similar fashion to terrestrial olivine tholeiite, increasing at low degrees of fractionation before decreasing at the later stages (Figure 11). These general characteristics also hold true for the “dry” path, but it shows more restricted variability in Mg/Si ratio. This trend shows that residual liquids evolving along both the “wet” and “dry” paths have higher Al/Si ratios than their respective parental liquids for any given degree of fractionation; therefore, Al/Si ratios of fractionally crystallized lavas on the Martian surface will have higher Al/Si ratios than those of their parental liquids.

4.2. Lithologic Diversity at the Base of the Martian Crust

[30] The variability in the surface lavas that arise from deep fractionation as a function of water content is also mirrored by variability in the nature of the cumulate lithologies left behind in the lower crust. The cumulate lithologies (represented by the bulk solids for each experiment) for both the “wet” and “dry” paths range from ultramafic to mafic in composition; however, the “wet” path crosses over from ultramafic to mafic (at the onset of feldspar crystallization) at a much higher degree of frac-

tionation (~75%) than along the “dry” path (~45%) (Figure 12). The mg#'s of the residual solids start out at ~70 and 68 for the “wet” and “dry” paths, respectively, and steadily decrease toward the bulk mg# with increasing degrees of fractionation. The rocktypes added to the base of the Martian crust via fractionation of a Humphrey-like primary magma are highly dependent on both the bulk starting water content of the parental melt and the extent of crystallization prior to liquid separation. Figure 12 shows the relationship between degree of fractionation and the nature of the lithology added to the base of the Martian crust for both the “dry” and “wet” paths (Figure 12A and 12B, respectively). The rocktypes indicated in Figure 12 represent the bulk modal mineralogy; they do not preclude the formation of monomineralic cumulus layering within the deep magma chambers.

4.3. Time-Dependent Stratification in the Upper and Lower Martian Crust

[31] The earliest post-magma ocean magmatism on Mars is likely represented by the most hydrous magmatism because any water remaining in the depleted mantle would partition strongly into melt. Without a mechanism for re-hydration (i.e., plate subduction), continued tapping of the same mantle source would result in a general dehydration trend in the magmas as the water is depleted in the source region upon repeated melt generation. Because of the major differences in liquid-line-of-descent between “wet” versus “dry” parental liquids, there could have been a dramatic shift in surface lithology compositions over time. This implies that any lithologies on the Martian surface today that are the product of fractional crystallization are more likely to represent lithologies

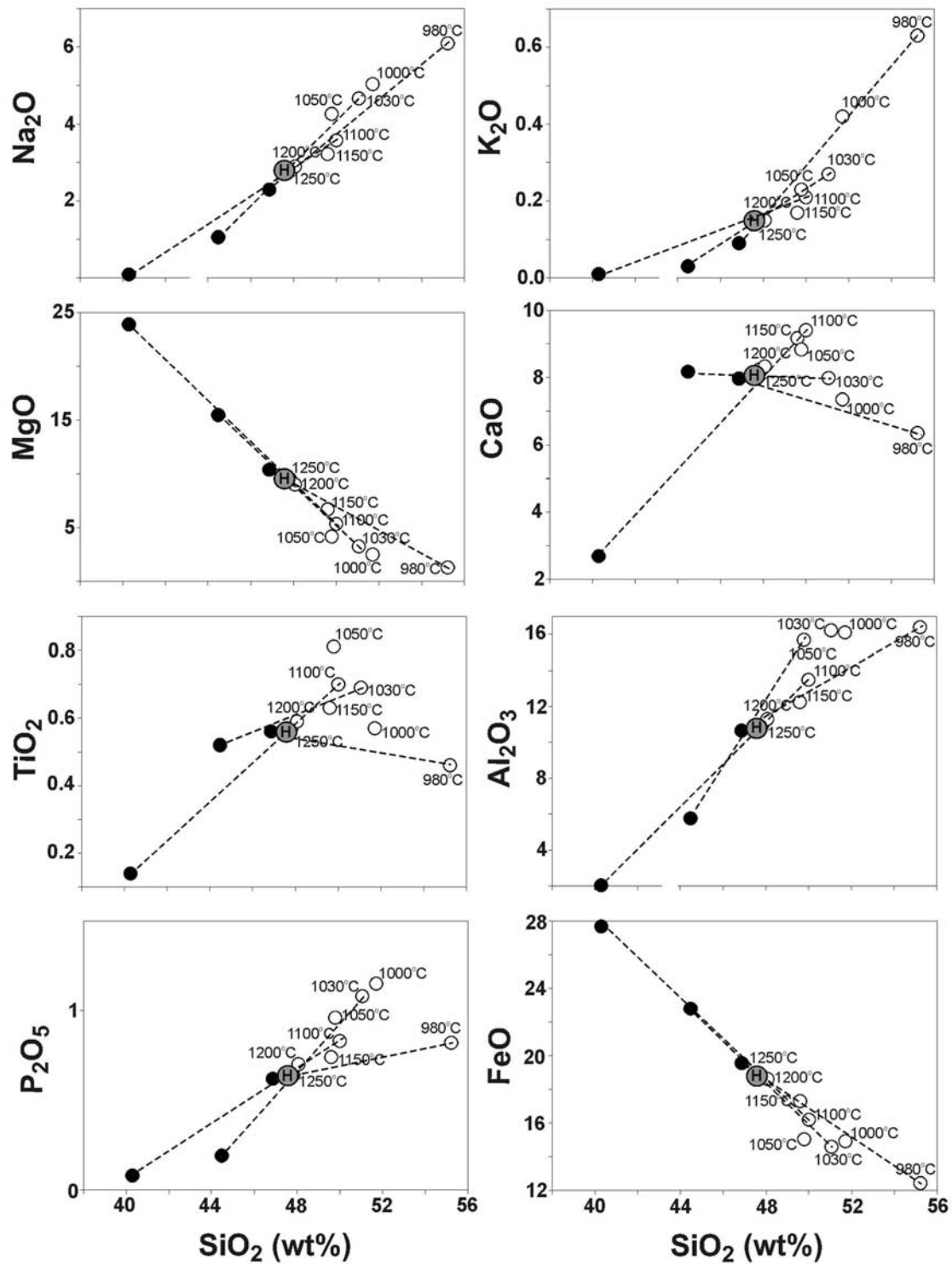
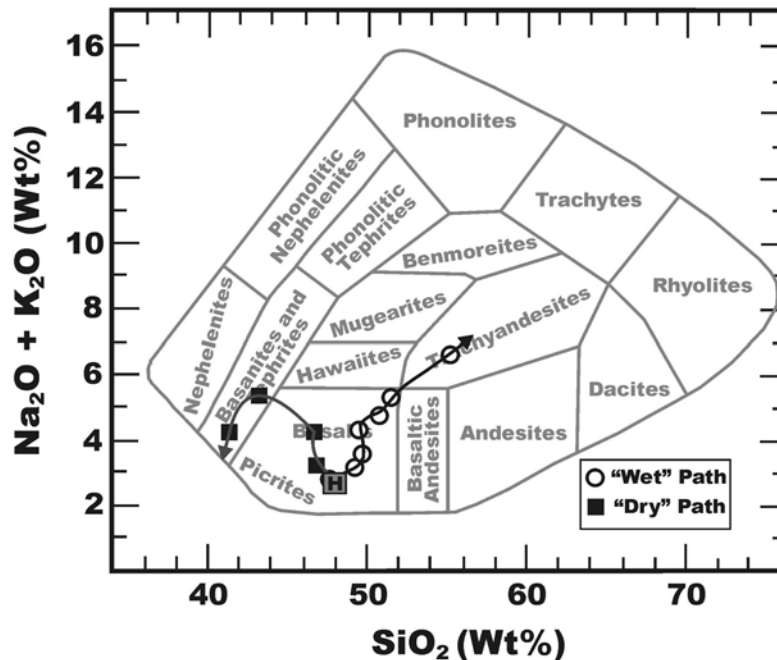


Figure 7. Harker-variation diagram for (open circles) residual liquids and (black circles) bulk solids from experiments on Humphrey (H) with 1.67 wt% bulk water at 9.3 kbar. Coexisting phases at each temperature are connected by dashed lines.

Table 8. Computed^a Bulk Residual Solid Compositions From Experiments on Hsynth Wet (1.67 wt% Bulk H₂O^b) at 9.3 kbar

Experiment (No.)	3.026	3.029	3.022	3.023	3.027	3.028	3.030	3.032
Temperature (°C)	1250	1200	1150	1100	1050	1030	1000	980
SiO ₂	0.00	26.3	34.5	40.3	43.5	44.2	45.6	46.2
TiO ₂	0.45	0.14	0.14	0.14	0.17	0.50	0.66	0.60
Al ₂ O ₃	9.26	3.05	1.90	2.03	2.36	5.87	7.86	10.1
Cr ₂ O ₃	56.7	16.4	4.67	2.82	1.79	1.27	0.87	0.54
FeO	25.9	26.5	29.1	27.7	25.5	22.5	20.5	19.0
MnO	0.20	0.26	0.46	0.33	0.35	0.34	0.35	0.39
MgO	7.11	27.0	28.8	23.9	19.3	15.4	12.8	10.9
CaO	0.25	0.21	0.33	2.69	6.72	7.98	8.03	8.41
Na ₂ O	0.04	0.01	0.01	0.09	0.18	1.15	1.66	2.18 ^c
K ₂ O	0.00	0.01	0.00	0.01	0.00	0.03	0.08	0.07
P ₂ O ₅	0.02	0.05	0.04	0.08	0.15	0.14	0.44	0.65
H ₂ O	0.00	0.00	0.00	0.00	0.00	0.40 ^d	0.68 ^d	0.68 ^d
F	0.00	0.00	0.00	0.00	0.00	0.42	0.73	0.56
Cl	0.00	0.00	0.00	0.00	0.00	0.02	0.04	0.05
-O = F + Cl	0.00	0.00	0.00	0.00	0.00	0.18	0.31	0.23
Total	99.9	99.9	100.0	100.1	100.0	100.1	100.0	100.1
mg# ^e	0.36	0.68	0.67	0.64	0.61	0.59	0.57	0.55

^aComputed from phase abundances.^bMeasured by FTIR.^cValue calculated from plagioclase that was corrected for Na-loss.^dCalculated based on crystal chemistry.^emg# = Molar Mg/(Mg + Fe²⁺) assuming an Fe²⁺/Fe_{Total} ratio of 0.85.**Figure 8.** Variation in total alkalis vs. silica in experimental residual liquids produced from Humphrey composition (H) liquid at 9.3 kbar under both “dry” (0.07 wt% bulk water; black squares) and “wet” (1.67 wt% bulk water; open circles) conditions. Arrows indicate the down-temperature direction. The rock classification scheme of Cox *et al.* [1984] is shown in the background.

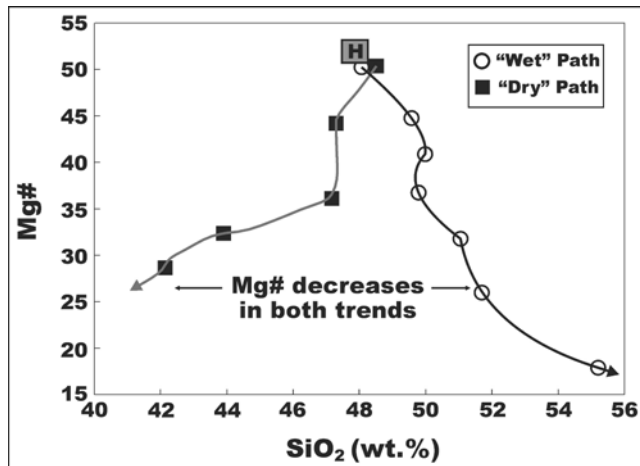


Figure 9. Variation in mg# (as defined in Tables 3 and 7) vs. silica in experimental residual liquids produced from Humphrey composition (H) liquid at 9.3 kbar under both “dry” (0.07 wt% bulk water; black squares) and “wet” (1.67 wt% bulk water; open circles) conditions. Arrows indicate the down-temperature direction.

along the “dry” trend, which means that the current Martian surface is more likely composed of basaltic to basaltic lithologies, which is consistent with mission-based observations of the Martian surface. Importantly, this does not preclude the existence of silica-rich lithologies below the surface, especially if Mars had a wet mantle early in its history. The relative thicknesses of the “wet-path” layer versus the “dry-path” layer would largely be a function of the water budget of the mantle at the respective mantle source and the degree of crystallization that took place before residual liquid separation.

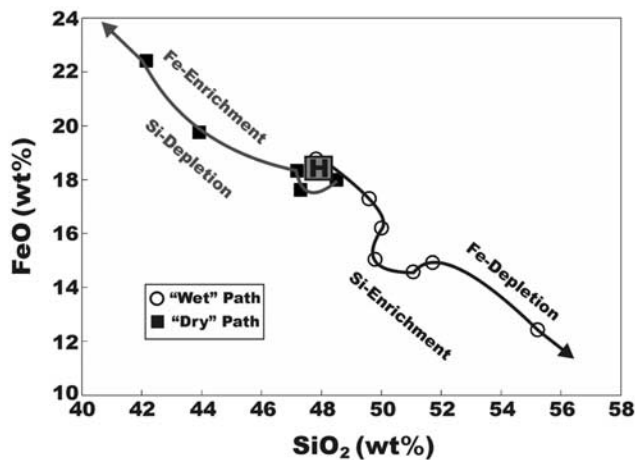


Figure 10. Variation in total iron (as FeOT) vs. silica in experimental residual liquids produced from Humphrey composition (H) liquid at 9.3 kbar under both “dry” (0.07 wt% bulk water; black squares) and “wet” (1.67 wt% bulk water; open circles) conditions. Arrows indicate the down-temperature direction.

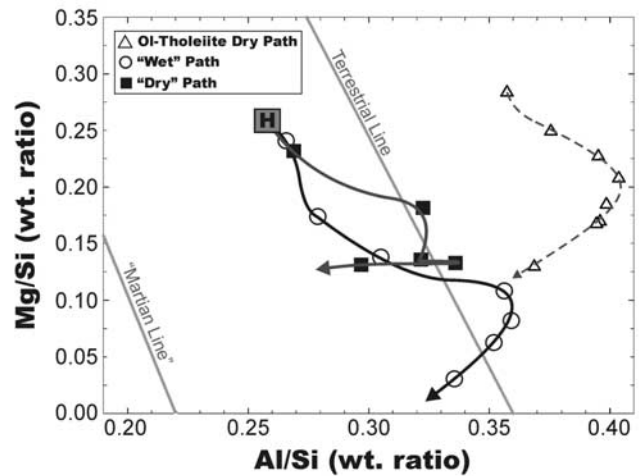


Figure 11. Mg/Si vs. Al/Si weight ratios of experimental residual liquids (adapted from *Filiberto et al.* [2006]) produced from Humphrey composition (H) liquid at 9.3 kbar under both “dry” (0.07 wt% bulk water; black squares) and “wet” (1.67 wt% bulk water; open circles) conditions. Arrows indicate the down-temperature direction. Residual liquids from crystallization of a terrestrial olivine tholeiite (open triangles) with 0.05 wt% bulk water and at 9.3 kbar pressure are shown for comparison. The geochemical fractionation lines of *Jagoutz et al.* [1979] for Earth and from *Wanke et al.* [1986] for Mars are also shown for comparison.

[32] The lower Martian crust would also undergo stratification because of the change in water budget over time. During the period of extensive hydrous magmatism, ultramafic rocks are likely added to the base of the crust, and, if sufficient fractionation took place before residual liquid separation, amphibole will be present in the lower crust. This amphibole could undergo dehydration melting upon the passage of younger, hotter, drier magmas and contribute Ca-Mg-Ti-rich hydrous melt to the surface or subsurface. The youngest portion of the lower crust, represented by the residual solids produced during fractionation of “dry” magmas, would likely be a mixture of mafic and ultramafic material, and instead of amphibole, plagioclase would be present if sufficient crystallization occurred prior to loss of residual liquid.

[33] The results of these experiments suggest that if drier magmas dominated the latest stages of magmatic activity of the planet, the present-day surface would be characterized by high Fe and low silica basaltic compositions. These compositions would be evolved with low mg#'s and would not reflect primary magmas or source regions with similarly low mg#'s. The variability in Al/Si ratio, iron-content, and silica-content of the evolving liquids during deep-seated fractionation points out the potential problems of using compositional data from surface rocks to access information about primitive liquid compositions and magmatic source regions. Such information may be further obscured by additional processes such as wallrock assimilation and mixing with the products of dehydration melting as the residual liquids ascend toward the surface.

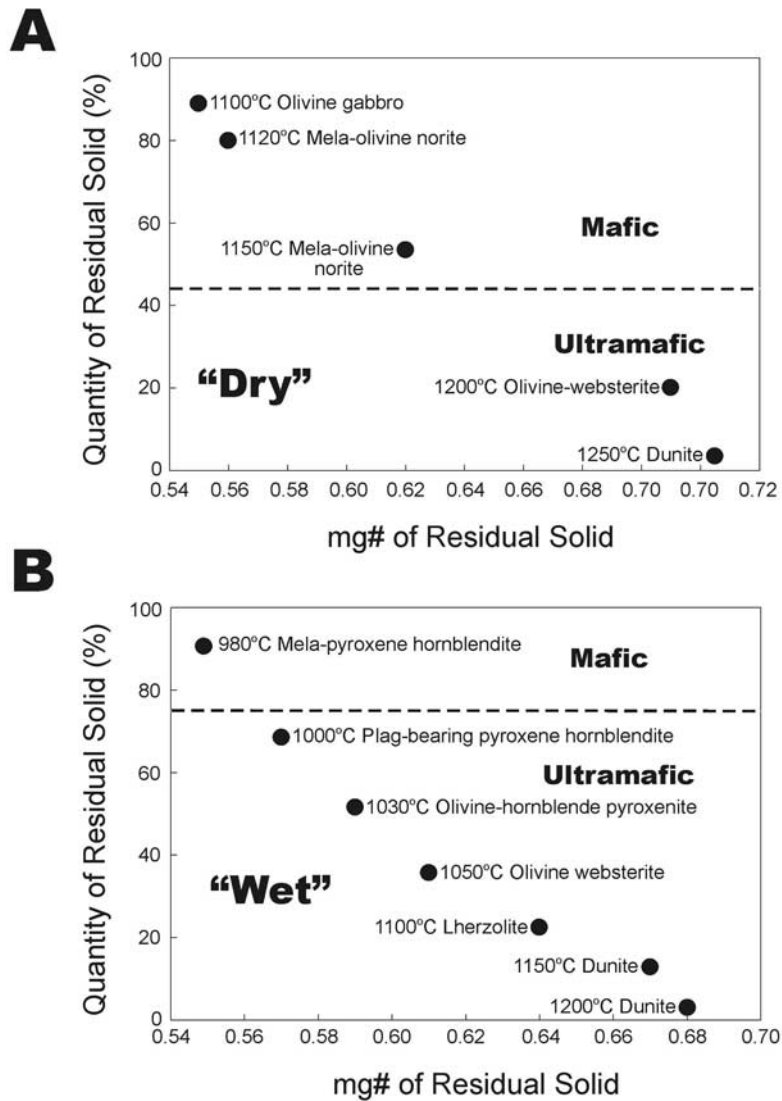


Figure 12. Abundance of residual solid (wt% of system, where the system consists of residual liquid + crystallized solid) vs. bulk mg# of the residual solids from experiments on the Humphrey composition at 9.3 kbar. Rock names are from the IUGS classification of ultramafic rocks and gabbroic rocks. (Pigeonite was recast into 2/3 orthopyroxene and 1/3 augite.) Boundaries (dashed lines) between mafic and ultramafic cumulate lithologies were placed where the cumulus assemblage was estimated to contain 10 modal % plagioclase. Rock types were determined from the mineral modes in Tables 3 and 7. (A) For experiments conducted with 0.07 wt% bulk water.

[34] **Acknowledgments.** We thank Charles Mandeville of the American Museum of Natural History for hours of assistance in using both the electron microprobe and the micro-FTIR instrument. We would also like to thank H. Y. McSween and an unnamed reviewer for insightful and thorough reviews of this paper. Financial support for this work was provided by NASA grant NNG04GM79G from the Mars Fundamental Research Program, awarded to Hanna Nekvasil, and Francis McCubbin was partially supported by a Graduate Assistance in Areas of National Need (GAANN) Fellowship.

References

- Albarede, F., et al. (1997), The geochemical regimes of Piton de la Fournaise volcano (Reunion) during the last 530,000 years, *J. Petrol.*, **38**, 171–201.
- Andersen, D. J., et al. (1993), Quilf—A Pascal program to assess equilibria among Fe-Mg-Mn-Ti oxides, pyroxenes, olivine, and quartz, *Comput. Geosci.*, **19**, 1333–1350.
- Bandfield, J. L., et al. (2004), Identification of quartzofeldspathic materials on Mars, *J. Geophys. Res.*, **109**, E10009, doi:10.1029/2004JE002290.
- Borg, L. E., et al. (1997), Constraints on Martian differentiation processes from Rb-Sr and Sm-Nd isotopic analyses of the basaltic shergottite QUE 94201, *Geochim. Cosmochim. Acta*, **61**, 4915–4931.
- Borg, L. E., et al. (2003), The age of Dar al Gani 476 and the differentiation history of the Martian meteorites inferred from their radiogenic isotopic systematics, *Geochim. Cosmochim. Acta*, **67**, 3519–3536.
- Brandon, A. D., et al. (2000), Re-Os isotopic evidence for early differentiation of the Martian mantle, *Geochim. Cosmochim. Acta*, **64**, 4083–4095.
- Breuer, D., and T. Spohn (2003), Early plate tectonics versus single-plate tectonics on Mars: Evidence from magnetic field history and crust evolution, *J. Geophys. Res.*, **108**(E7), 5072, doi:10.1029/2002JE001999.
- Carr, M. J. (2002), *IgPet for Windows*, Terra Softa Inc., Somerset, N. J.
- Christensen, P. R., et al. (2005), Evidence for magmatic evolution and diversity on Mars from infrared observations, *Nature*, **436**, 504–509.
- Clark, B. C., et al. (2005), Chemistry and mineralogy of outcrops at Meridiani Planum, *Earth Planet. Sci. Lett.*, **240**, 73–94.
- Cox, K. G. (1972), The Karoo volcanic cycle, *J. Geol. Soc. (London)*, **128**, 311–336.
- Cox, K. G., et al. (1984), *The Interpretation of Igneous Rocks*, 4th ed., 450 pp., George Allen & Unwin, London.
- Eugster, H. P., and G. B. Skippen (1967), Igneous and metamorphic reactions involving gas equilibria, in *Researches in Geochemistry*, edited by P. H. Abelson, pp. 492–520, John Wiley, New York.
- Filiberto, J. (2008), Experimental constraints on the parental liquid of the Chassigny meteorite: A possible link between the Chassigny meteorite and a Martian Gusev basalt, *Geochim. Cosmochim. Acta*, **72**, 690–701.
- Filiberto, J., and H. Nekvasil (2003), Linking tholeiites and silica-undersaturated alkalic rocks: An experimental study, *GSA Abstracts with Programs*, **34**, 258–16.
- Filiberto, J., et al. (2006), The Mars/Earth dichotomy in Mg/Si and Al/Si ratios: Is it real?, *Am. Mineral.*, **91**, 471–474.
- Foley, C. N., et al. (2005), The early differentiation history of Mars from W-182-Nd-142 isotope systematics in the SNC meteorites, *Geochim. Cosmochim. Acta*, **69**, 4557–4571.
- Gellert, R., et al. (2006), Alpha particle X-ray spectrometer (APXS): Results from Gusev crater and calibration report, *J. Geophys. Res.*, **111**, E02S05, doi:10.1029/2005JE002555.
- Greenwood, J. P. (2005), Chlorine-rich apatites in SNCs: Evidence for magma-brine interactions on Mars?, *Meteorit. Planet. Sci.*, **40**, A60.
- Harper, C. L., et al. (1995), Rapid accretion and early differentiation of Mars indicated by Nd-142 Nd-144 in Snc meteorites, *Science*, **267**, 213–217.
- Jagoutz, E., et al. (1979), The abundances of major, minor, and trace elements in the Earth's mantle as derived from primitive ultramafic nodules, in *Proceedings of the 10th Lunar and Planetary Science Conference*, *Geochim. Cosmochim. Acta Suppl.* **11**, 2031–2050.
- Kleine, T., et al. (2002), Rapid accretion and early core formation on asteroids and the terrestrial planets from Hf-W chronometry, *Nature*, **418**, 952–955.
- Kleine, T., et al. (2004), Hf-182-W-182 isotope systematics of chondrites, eucrites, and Martian meteorites: Chronology of core formation and early mantle differentiation in Vesta and Mars, *Geochim. Cosmochim. Acta*, **68**, 2935–2946.
- LeBas, M. J., et al. (1986), A chemical classification of volcanic rocks based on the total alkali silica diagram, *J. Petrol.*, **27**, 745–750.
- Lee, D. C., and A. N. Halliday (1997), Core formation on Mars and differentiated asteroids, *Nature*, **388**, 854–857.
- MacDonald, G. A. (1968), Composition and origin of Hawaiian lavas, *Mem.-Geol. Soc. Am.*, **116**, 477–522.
- Mandeville, C. W., et al. (2002), Determination of molar absorptivities for infrared absorption bands of H₂O in andesitic glasses, *Am. Mineral.*, **87**, 813–821.
- McCubbin, F. M., and H. Nekvasil (2008), Maskelynite-hosted apatite in the Chassigny meteorite: Insights into late-stage magmatic volatile evolution in Martian magmas, *Am. Mineral.*, **93**, 676–684.
- McLennan, S. M. (2001), Crustal heat production and the thermal evolution of Mars, *Geophys. Res. Lett.*, **28**, 4019–4022.
- McLennan, S. M. (2003), Large-ion lithophile element fractionation during the early differentiation of Mars and the composition of the Martian primitive mantle, *Meteorit. Planet. Sci.*, **38**, 895–904.
- McSween, H. Y., and R. P. Harvey (1993), Outgassed water on Mars—Constraints from melt inclusions in Snc meteorites, *Science*, **259**, 1890–1892.
- McSween, H. Y., et al. (2006a), Alkaline volcanic rocks from the Columbia Hills, Gusev crater, Mars, *J. Geophys. Res.*, **111**, E09S91, doi:10.1029/2006JE002698.
- McSween, Y., et al. (2006b), Characterization and petrologic interpretation of olivine-rich basalts at Gusev Crater, Mars, *J. Geophys. Res.*, **111**, E02S10, doi:10.1029/2005JE002477.
- Monders, A. G., et al. (2007), Phase equilibrium investigations of the Adirondack class basalts from the Gusev plains, Gusev crater, Mars, *Meteorit. Planet. Sci.*, **42**, 131–148.
- Morrison, J. (1991), Compositional constraints on the incorporation of Cl into amphiboles, *Am. Mineral.*, **76**, 1920–1930.
- Naumann, T. R., and D. J. Geist (1999), Generation of alkalic basalt by crystal fractionation of tholeiitic magma, *Geology*, **27**, 423–426.
- Nekvasil, H., et al. (2004), The origin and evolution of silica-saturated alkalic suites: An experimental study, *J. Petrol.*, **45**, 693–721.
- Nekvasil, H., et al. (2007), Alkalic parental magmas for the chassignites?, *Meteorit. Planet. Sci.*, **42**, 979–992.
- Norman, M. D. (1999), The composition and thickness of the crust of Mars estimated from rare earth elements and neodymium-isotopic compositions of Martian meteorites, *Meteorit. Planet. Sci.*, **34**, 439–449.
- Nyquist, L. E., et al. (2001), Ages and geologic histories of Martian meteorites, *Space Sci. Rev.*, **96**, 105–164.
- Rogers, A. D., and P. R. Christensen (2007), Surface mineralogy of Martian low-albedo regions from MGS-TES data: Implications for upper crustal evolution and surface alteration, *J. Geophys. Res.*, **112**, E01003, doi:10.1029/2006JE002727.
- Scoates, J. S., et al. (1999), Fractional crystallization experiments on a candidate parental magma to anorthosite, *Eos Trans., AGU*, **80**, F1096.
- Squyres, S. W., et al. (2006), Rocks of the Columbia Hills, *J. Geophys. Res.*, **111**, E02S11, doi:10.1029/2005JE002562.
- Taylor, G. J., et al. (2006), Bulk composition and early differentiation of Mars, *J. Geophys. Res.*, **111**, E03S10, doi:10.1029/2005JE002645.
- Taylor, S. R. (2001), *Solar System Evolution: A New Perspective*, 2nd ed., 460 pp., Cambridge Univ. Press, New York.
- Thompson, R. N. (1975), Primary Basalts and Magma Genesis. 2: Snake River Plain, Idaho, USA, *Contrib. Mineral. Petrol.*, **52**, 213–232.
- Wanke, H., et al. (1986), ALHA 77005 and on the chemistry of the Shergotty parent body (Mars), *Lunar Planet. Sci.*, 919–920.
- Webster, J. D., and C. R. Rebbert (1998), Experimental investigation of H₂O and Cl⁻ solubilities in F-enriched silicate liquids; implications for volatile saturation of topaz rhyolite magmas, *Contrib. Mineral. Petrol.*, **132**, 198–207.
- Webster, J. D., et al. (1999), Chloride and water solubility in basalt and andesite melts and implications for magmatic degassing, *Geochim. Cosmochim. Acta*, **63**, 729–738.
- Whitaker, M. L., et al. (2005), Potential magmatic diversity on Mars, paper presented at Proceedings of the Lunar and Planetary Science Conference XXXVI, Houston, TX, Abstract 1440.
- Whitaker, M. L., et al. (2007), The role of pressure in producing compositional diversity in intraplate basaltic magmas, *J. Petrol.*, **48**, 365–393.
- Wieczorek, M. A., and M. T. Zuber (2004), Thickness of the Martian crust: Improved constraints from geoid-to-topography ratios, *J. Geophys. Res.*, **109**, E01009, doi:10.1029/2003JE002153.
- Wright, J. B. (1970), High pressure phases in Nigerian Cenozoic lavas, distribution and geotectonic setting, *Bull. Volcanol.*, **34**, 833–847.
- Yin, Q. Z., et al. (2002), A short timescale for terrestrial planet formation from Hf-W chronometry of meteorites, *Nature*, **418**, 949–952.

S. M. Elardo, Institute of Meteoritics, MSC03 2050, 1 University of New Mexico Albuquerque, NM 87131-0001, USA.

A. D. Harrington, D. H. Lindsley, F. M. McCubbin, and H. Nekvasil, Department of Geosciences, Stony Brook University, Stony Brook, NY 11794-2100, USA. (fmccubbi@ic.sunysb.edu)